Summer 2014

Transverse compression of high-performance ballistic fibers

Zherui Guo
Purdue University

PURDUE UNIVERSITY
GRADUATE SCHOOL
Thesis/Dissertation Acceptance

This is to certify that the thesis/dissertation prepared

By Zherui Guo

Entitled
Transverse Compression of High-Performance Ballistic Fibers

For the degree of Master of Science in Aeronautics and Astronautics

Is approved by the final examining committee:

Weinong Chen

Vikas Tomar

Jeffrey P. Youngblood

To the best of my knowledge and as understood by the student in the *Thesis/Dissertation Agreement. Publication Delay, and Certification/Disclaimer (Graduate School Form 32)*, this thesis/dissertation adheres to the provisions of Purdue University's "Policy on Integrity in Research" and the use of copyrighted material.

Weinong Chen

Approved by Major Professor(s): _____

_____

Approved by: Weinong Chen 05/28/2014

Head of the Department Graduate Program Date

TRANSVERSE COMPRESSION OF HIGH PERFORMANCE BALLISTIC FIBERS

A Thesis

Submitted to the Faculty

of

Purdue University

by

Zherui Guo

In Partial Fulfillment of the

Requirements for the Degree

of

Master of Science in Aeronautics and Astronautics

August 2014

Purdue University

West Lafayette, Indiana

ACKNOWLEDGMENTS

I would like to take this opportunity to thank my academic advisor and mentor Prof. Weinong Chen, without whom this thesis would not exist. He has been a major source of support and guidance for this study, and his enthusiasm for research definitely spreads to his students. Next, I would like to thank Dr. Casem, who contributed a large part of the high-rate experimental setup discussion and results. I would also like to thank my committee members, Prof. Vikas Tomar and Prof. Jeffrey Youngblood.

My gratitude also extends to my fellow labmates, without whose constant banter and exchange of ideas this study would not have gone as smoothly. In particular, I would like to thank Matthew Hudspeth and Benjamin Claus, who helped me brainstorm ideas and solutions when obstacles arose; Jianzhuo Sun, who helped me immensely with the scanning electron microscope images; and Niranjan Parab, who helped me get more in-depth into finite-element analysis using ABAQUS.

Finally, to my family, who have given me their constant moral support in whatever I do, especially during difficult and stressful times. I may not have seen them for years but hopefully this makes up for my absence.

TABLE OF CONTENTS

LIST OF TABLES

LIST OF FIGURES

Figure Page

SYMBOLS

F	transverse load
ε	strain
d	fiber diameter
Δd	radial deformation of fiber
E	Young's modulus
E_1	transverse Young's modulus
E_3	longitudinal Young's modulus
L	fiber gage length
r	fiber radius
s_{11}	$1/E_1$
s_{12}	$-\frac{\nu_{12}}{E_{12}}$
s_{13}	$1/E_{13}$
σ	stress

ABBREVIATIONS

NDI	Normal Displacement Interferometer
PPTA	para-phenyleneterepthalamide
UHMWPE	ultra-high-molecular-weight polyethylene
TDI	Transverse Displacement Interferometer

ABSTRACT

Guo, Zherui M.S.A.A., Purdue University, August 2014. Transverse Compression of High Performance Ballistic Fibers. Major Professor: Weinong Chen.

High performance ballistic fibers have been in use for decades, specifically in protective applications against ballistic impact such as bulletproof vest layers and aircraft turbine engine fragmentation barriers. These high performance fibers have extremely high strength-to-weight ratios and high moduli of elasticity in the axial direction, making them extremely suitable for high impact situations. In particular, para-phenyleneterephthalamide (PPTA for short) fibers such as Kevlar® and ultra-high-molecular-weight polyethylene fibers such as Dyneema® are amongst the more popular high performance fibers in today's world. While the longitudinal mechanical response of these fibers have been extensively researched, their transverse mechanical response is still not well-understood, even though most ballistic impact events occur in the radial direction of these fibers (especially in woven structures).

The method of determining the transverse mechanical response of Kevlar® KM2 and Dyneema® SK76 fibers was improved upon from previous versions of single fiber compression tests. Two fibers were laid parallel and compressed between two tool steel platens. The new experimental setup ensures that the individual fibers are being compressed evenly along the length and that the platens are parallel during compression. Nominal stress-strain curves were obtained for quasi-static loading of both types of fibers.

Proper calibration was also performed to ensure the accuracy of the obtained nominal stress-strain results. Using finite element analysis with ABAQUS, the quasi-static compression behavior was simulated and compared with experimental results.

Scanning electron microscopy was also performed to ensure uniform compression of the fibers.

To evaluate the rate effects on the transverse behavior, high-rate transverse compression experiments were also performed using a 127 μm diameter miniature Kolsky bar loading on single-fiber specimens to obtain the corresponding stress-strain response of these high performance fibers at high rates of deformation.

1. Introduction

1.1 High-Performance Fibers

High-performance materials are typically characterized by certain specific criteria, most notably for their excellent properties such as thermal resistance, mechanical strength, low specific density, high thermal, electrical, or sound insulation, as well as resistance to destructive conditions such as flames or chemicals [1].

More specifically, high-performance fibers have long been in use to strengthen and reinforce other materials. While most of the earlier fiber materials were metallic, one of the first high-performance fibers was made of glass, which had a strength of about 2 GPa [2]. These glass fibers were mainly used in composites, resulting in a lightweight and yet high-strength material with many useful applications. One well-known example of a popular composite material made from glass fibers is fiberglass, which is typically made by coating woven fiberglass fabrics with a resin. Fiberglass is still in use today in many commercial products such as boats, hobby aircraft, and surfboards.

Carbon fibers were the next step in composite technology, and were first developed by Roger Bacon in 1958. Carbon fibers, by themselves, exhibit higher strength-to-weight ratio compared to glass fibers. The popularity of carbon fibers increased as carbon-fiber-reinforced composite materials became more widespread in commercial applications, such as automotive and aircraft parts. Even today, carbon-fiber composites are still widely-used, with particular focus on the recently-developed Boeing 787 Dreamliner, which contains approximately 35 tons of carbon-fiber-reinforced polymer. Carbon fibers have been shown to be stronger and more rigid, although the disadvantage of carbon fibers is their brittleness [3].

With the advent of solvent-based spinning technology, modern polymer fibers are able to surpass the material properties exhibited by their predecessors. Two popular polymers used in today's ballistic fiber industry are para-phenyleneterepthalamide (PPTA) and ultra-high-molecular-weight polyethylene (UHMWPE). The properties of these constituent fibers play an important role in determining the ballistic performance of the yarns and fabrics that are composed of these fibers. These polymer fibers are spun via extrusion of the polymers in a liquid state (typically melted or dissolved in a solvent) through a spinneret to form a long, continuous filament. This process is also known as wet spinning. However, the spinning and drawing process is complicated and an in-depth analysis of the different methods of drawing these fibers is not within the scope of this thesis, and therefore only the methods of synthesis and processing for the ballistic fibers used in this study (namely Kevlar® and Dyneema®) will be provided in detail.

1.1.1 Kevlar® KM2

Kevlar® is one of the more popular para-Aramid fibers in use in the market right now, with other examples being Nomex® (also by Du Pont), as well as Technora® and Twaron®, both of which are made by Teijin. It was first discovered by Stephanie Kwolek from DuPont in 1965, then further developed in the 1970's and continuously improved on till this day. The classical synthesis of Kevlar fibers starts with the low temperature poly-condensation of *p*-phenylene diamine (PPD) and terapthaloyl chloride (TCl) [4].

Para-Aramid fibers belong to a class of materials called liquid crystalline polymers, and in a solution form, these para-Aramid polymers can aggregate to form organised clusters compared to other conventional flexible polymers, which form random coils in a solution (Figure 1.3). This is due to the rigid rod-like structures of the polymers, which is the main factor in determining the strength of the resulting polymer fiber. These PPTA chains are relatively short, with a polymer mass average molecular

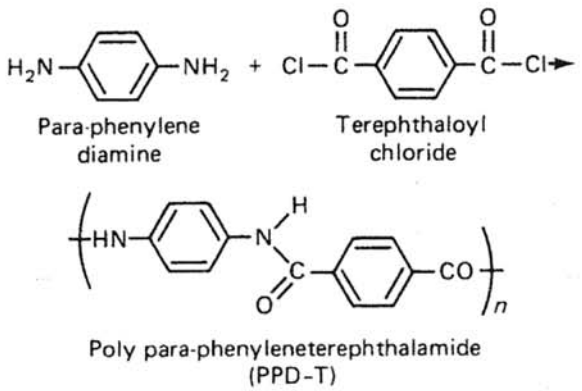

Figure 1.1. Synthesis of para-Aramid [5].

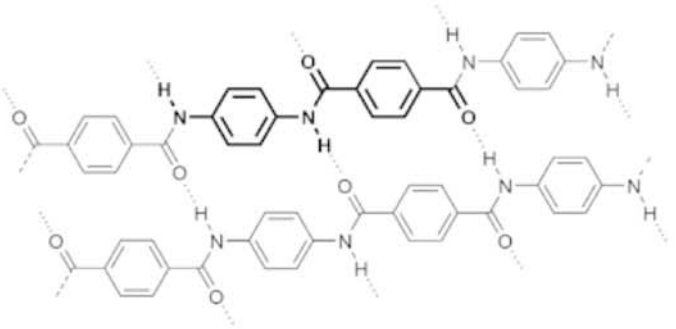

Figure 1.2. Structure of para-Aramid, with monomer highlighted in bold [6].

weight of 31,400 - 48,350 [7]. Due to their molecular structure, para-Aramids also have relatively high bending stiffness as the polymer chains do not fold easily.

The PPD-T solution in a concentrated sulfuric acid solvent is then extruded through a spinneret and then drawn through an air gap. During this process, the liquid crystalline micro-structures as in Figure 1.3(b) may orient and align in the flow direction. This alignment results in a high anisotropy of these fibers, and further high-temperature processing can further increase the orientations of the crystalline structures, thereby resulting in a higher modulus and other properties. Depending on the process involved in manufacturing the Kevlar fibers, several grades of Kevlar fibers with slightly differing properties can be produced. A brief summary of the different Kevlar types and their applications is given in Table 1.1.1.

Table 1.1 Properties and applications of several popular Kevlar® grades [8].

Grade	Properties	Applications
Kevlar 29	High strength	Industrial applications such as ropes and cables, cut-resistant gloves
Kevlar 49	High modulus	Fiber optics, ropes and cables, aerospace applications
Kevlar 119	Higher elongation, fatigue-resistant	Rubber goods such as tires, automotive belts, and hoses
Kevlar 129	Lightweight, high-tenacity	Life protection accessories, ropes and cables, high-pressure hoses
KM2	High tenacity, high toughness, finer-denier	Military and law-enforcement applications such as helmets and protective vests

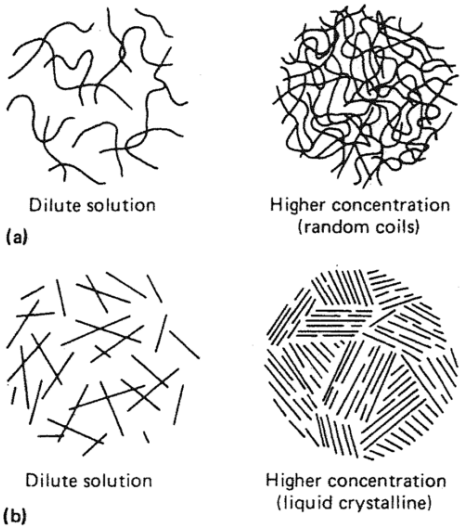

Figure 1.3. Arrangement of polymers in solvent for (a) conventional polymers, and (b) para-Aramid polymers [5].

In particular, Kevlar® KM2 fibers are typically used in ballistic applications due to their high strength-to-weight ratio, relatively high resistance to chemical and environmental exposure, and low thermal conductivity. These properties not only make it useful for protective applications such as bulletproof vests and jackets, but also for high-impact explosive conditions such as turbine engine fragmentation barriers in aircraft.

1.1.2 Dyneema® SK76

The other commonly-used polymer in today's industry is polyethylene, more specifically ultra-high molecular weight polyethylene (UHMWPE). Two of the well-known UHMWPE products are Dyneema® from DSM and Spectra® from Honeywell. UHMWPE fibers have replaced Aramid fibers in certain applications due to better resistance to degradation [9]. Compared to para-Aramid fibers, UHMWPE does not require extremely toxic or abrasive chemical solvents to produce, thereby contributing to their increasing popularity.

PPTA polymers are known to exhibit bending stiffness due to their rigid rod-like structure in small clusters, which also provides them with the necessary strength. Polyethylene, in contrast, is much more flexible due to its long chains with relatively weak transverse bonds. Polyethylene as a polymer has been in use for a long time, especially in the form of low-density polyethylene (LDPE) used in plastic bags and cartons, and high-density polyethylene (HDPE) used in plastic bottles and piping.

On the other hand, UHMWPE derives its strength from the van der Waal's forces between its extremely long chains of molecules. These van der Waal's forces, although weak individually, become significant when multiplied along the length of these polymers. The resulting structure is therefore highly-resistant to shearing between molecule chains, thereby accounting for their high longitudinal yield strength.

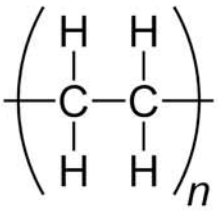

Figure 1.4. Structure of UHMWPE, with n typically greater than 10,000.

Due to this molecular structure, polyethylene molecules are much more flexible compared to PPTA polymers without sacrificing strength. The flexibility stems from their simple monomers: while PPTA molecules consist of large aromatic rings which prohibit excessive bending of the polymer chain, UHMWPE molecules consist of simple monomers which allow for a high degree of flexibility.

While other methods of processing UHMWPE were developed much earlier, gel-spinning technology wasn't in use till much later. Using a high-temperature solution of UHMWPE, the solution is then cooled to allow crystallization. The cooling allows polymer crystals to form in the solution, thereby obtaining a gel [2, 10]. This UHMWPE gel is then extruded through a spinneret, and then drawn either by stretching the fiber in a hot-air oven and removing the solvent at the simultaneously, or by

Table 1.2 Properties and applications of several popular Dyneema® grades [11].

Grade	Properties	Applications
HB26	High strength, lightweight	Armored vehicles, helmets
HB50	High stopping power, lightweight	Helmets, vehicle armor, high-velocity fragment barriers
SB71	High strength, lightweight	Bullet-resistant vests
SK75	High strength, lightweight	Ropes, lines, cables, and fishing nets
SK76	High modulus, lightweight	Military applications

drying the gel filaments at room temperature before removing any remaining solvent with ethanol. The gel fibers are then finally quenched in a water bath. This method of gel-spinning results in a highly-oriented anisotropic fiber with excellent longitudinal tensile properties. Similarly, by varying the processing of manufacturing, different grades of Dyneema® can be produced. A brief summary of the different Dyneema® grades and their applications are given below in Table 1.1.2.

1.2 Transverse Characterization of High-Performance Fibers

1.2.1 Anisotropy of High-Performance Fibers

For the mechanical response of a solid, Hooke's Law can be written in a compliance matrix form with the necessary material constants such as the Poisson's ratio and modulus in that direction. In particular, for a transversely isotropic solid such as a

fiber, the compliance matrix can be simplified to just five material constants defined in Equation 1.1 below [12].

$$\begin{Bmatrix} \varepsilon_{11} \\ \varepsilon_{22} \\ \varepsilon_{33} \\ \varepsilon_{23} \\ \varepsilon_{31} \\ \varepsilon_{12} \end{Bmatrix} = \begin{bmatrix} s_{11} & -\nu_{21}s_{11} & -\nu_{31}s_{33} & 0 & 0 & 0 \\ -\nu_{21}s_{11} & s_{11} & -\nu_{31}s_{33} & 0 & 0 & 0 \\ -\nu_{31}s_{33} & -\nu_{31}s_{33} & s_{33} & 0 & 0 & 0 \\ 0 & 0 & 0 & s_{23} & 0 & 0 \\ 0 & 0 & 0 & 0 & s_{23} & 0 \\ 0 & 0 & 0 & 0 & 0 & 2(1+\nu_{21})s_{11} \end{bmatrix} \begin{Bmatrix} \sigma_{11} \\ \sigma_{22} \\ \sigma_{33} \\ \sigma_{23} \\ \sigma_{31} \\ \sigma_{12} \end{Bmatrix} \tag{1.1}$$

where s and ν (also defined previously in the list of symbols) are the reciprocal of their corresponding modulus and Poisson's ratios in a particular direction respectively.

While the longitudinal properties (s_{33}) and mechanical response of highly-anisotropic fibers have already been extensively researched and experimented on, the transverse mechanical response (s_{11}) of these fibers have garnered relatively little attention and are therefore not as well-understood, despite the fact that nearly all impact and applications of these fabric structures are from out-of-plane or transverse directions. Several methods of characterizing the transverse mechanical properties have been developed as early as the 1970's, and many numerical and analytical models have followed suit as well.

1.2.2 Hertzian Contact Theory

Hertzian contact analysis [13] is an oft-used analytical model for determining the elastic modulus of fibers to a certain extent, particularly in the case of a circular cross-section in contact with two flat surfaces, as in Figure 1.5.

As the fiber of undeformed radius r gets compressed by a radial force F, the total contact width $2b$ increases. The main assumption of this Hertzian contact problem is that the width of the contact zone $2b$ is extremely small compared to the dimensions of the body in question, in this case the radius of the fiber r. In particular, Pinnock,

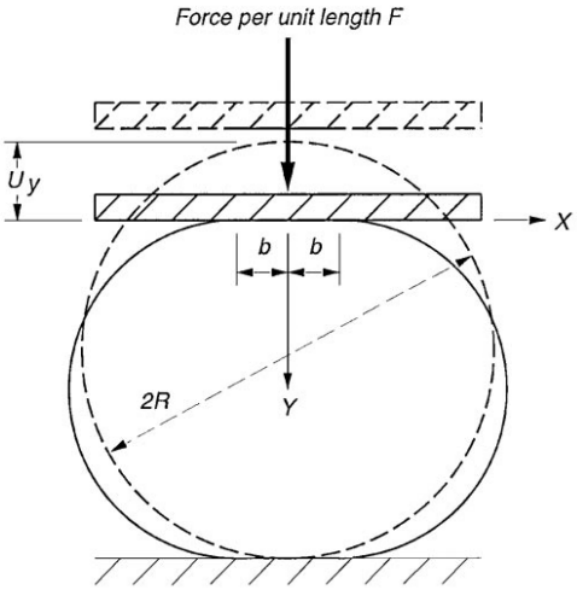

Figure 1.5. Using Hertzian contact theory between a circle and two flat surfaces to calculate the true stress and strain of the compressed fiber [14].

Ward, and Wolfe [15] considered this problem as the frictionless compression of an elastic cylinder by two concentrated loads on both ends of the fiber diameter. The total transverse deformation of the fiber (or platen displacement) is therefore given by 1.2

$$U_y = F\left[\left(\frac{4}{\pi} - 1\right)\left(s_{11} - \frac{s_{13}^2}{s_{33}}\right) - \left(s_{12} - \frac{s_{13}^2}{s_{33}}\right)\right] \tag{1.2}$$

Assuming transverse radial isotropy of the material and under plane strain compression, the fiber material properties such as the transverse elastic modulus and Poisson's ratio could be subsequently obtained from the experimental data. The contact width b is subsequently calculated using the equation

$$b^2 = \frac{4Fr}{\pi}\left(s_{11} - \frac{s_{11}^2}{s_{33}}\right) \tag{1.3}$$

It is then apparent that due to the increase in contact width b during compression, the true stress during transverse loading actually changes, leading to complexity during calculation.

However, due to the main assumptions used in the solution of the Hertzian contact problem, the analytical solution becomes invalid when the contact width $2b$ is significant large in comparison to the radius of the fiber. The Hertzian contact method is therefore only useful for calculating the initial transverse modulus of the fiber before the onset of plastic deformation (typically around 4% strain).

1.2.3 Single-Fiber Transverse Compression

A single fiber compression method to determine the transverse elastic modulus of anisotropic fibers was developed by Hadley, Ward, and Ward as early as 1965 [16]. In the study, polyethylene terephthalate, polypropylene, and nylon test monofilaments were tested for their transverse elastic modulus and transverse Poisson's ratio.

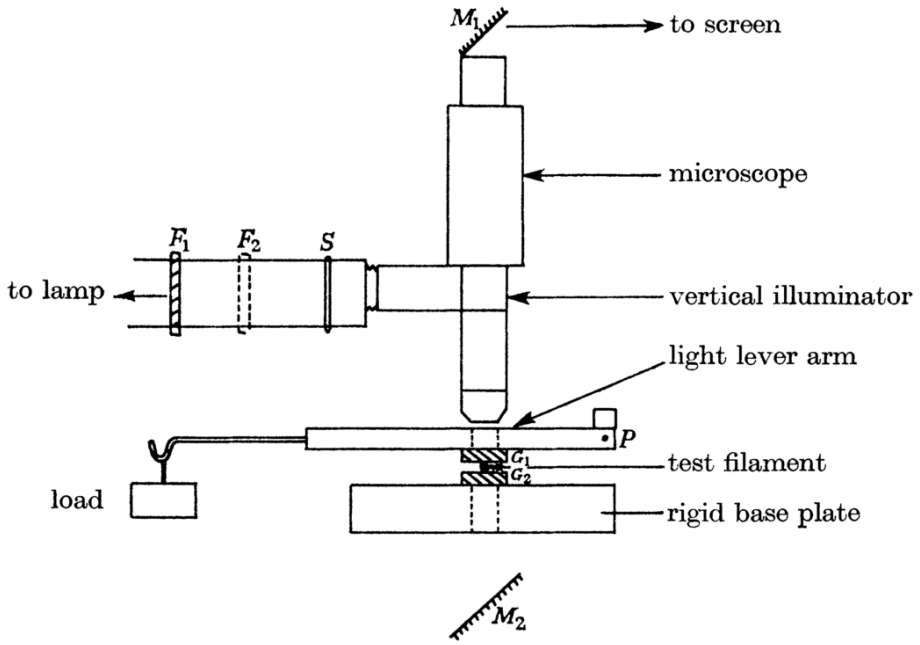

Figure 1.6. Transverse compression setup by Hadley et al. using interference fringes to determine the fiber contact width [16].

These monofilaments were sandwiched between two parallel glass or quartz plates, and a load was subsequently applied on the fiber via a lever arm with weights hanging on one end. The corresponding contact width of the fiber with the glass platen at different load levels during compression was monitored under a microscope using interference fringe patterns.

Three years later, Morris [17] improved upon Hadley et al's setup to measure nylon, acrylic, and Rayon fibers. The physical basis behind both setups is similar, however, Morris chose to compress the fibers using horseshoe weights on a stack of glass plates where the fibers are sandwiched in between. The micrometer is then lowered until it touches the glass plates, thereby measuring the transverse deformation of these fibers.

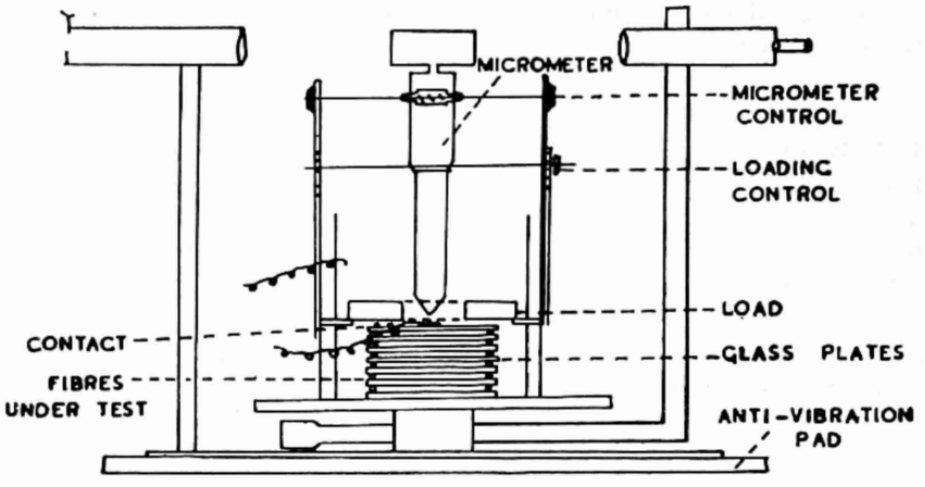

Figure 1.7. Transverse compression setup by Morris using a micrometer to measure the displacement up to the point where it contacts the top glass plate [17].

1.2.4 Automated Single-Fiber Transverse Compression

The Hertzian contact theory, although slightly modified, is still in use for the calculation of the transverse elastic moduli of highly-oriented anisotropic fibers. However, transverse compression methods have been improved upon since Hadley et al.'s ini-

tial experiment. In 1990, Kawabata [18] performed similar transverse compression experiments on aramid fibers by laying out a single fiber on a smooth, flat steel bed (Figure 1.8). The top plane, similar to an indenter, was driven by an electromagnetic power driver to compress the fiber and a force transducer to detect the amount of force being applied. A linear differential transformer connected to the driver rod detects the displacement of the indenter plane as it moves downward to compress the fiber.

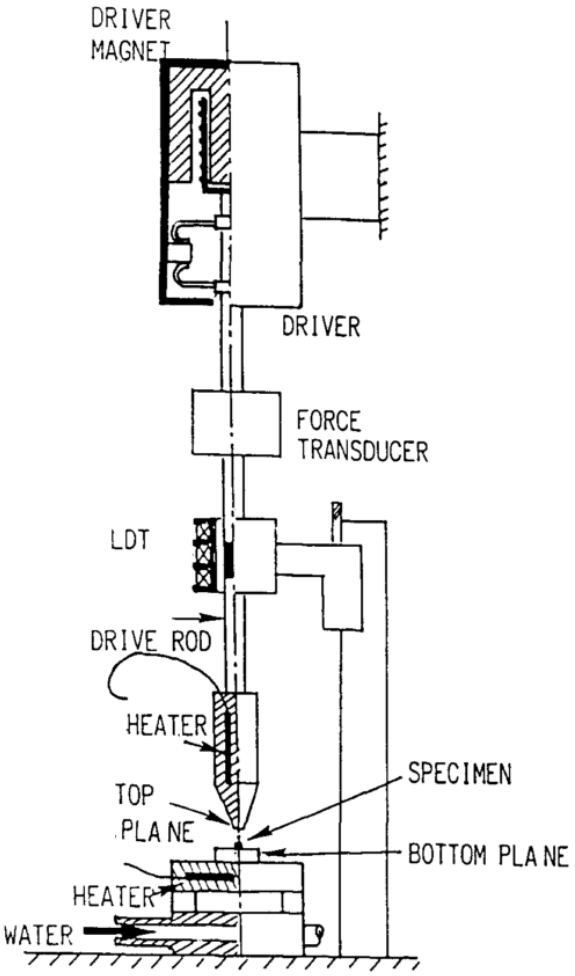

Figure 1.8. Automated transverse compression setup by Kawabata [18].

The main advantage of this setup is its ability to directly measure extremely small changes in initial elastic deformation because of the high resolution of the equipment,

as well as more accurately control and measure the amount of force applied on the fiber, rather than indirectly measure the contact width using interference fringes. Due to the success of this experimental setup, subsequent fiber transverse compression experiments [14, 19] were mostly based on slight modifications of Kawabata's experimental setup.

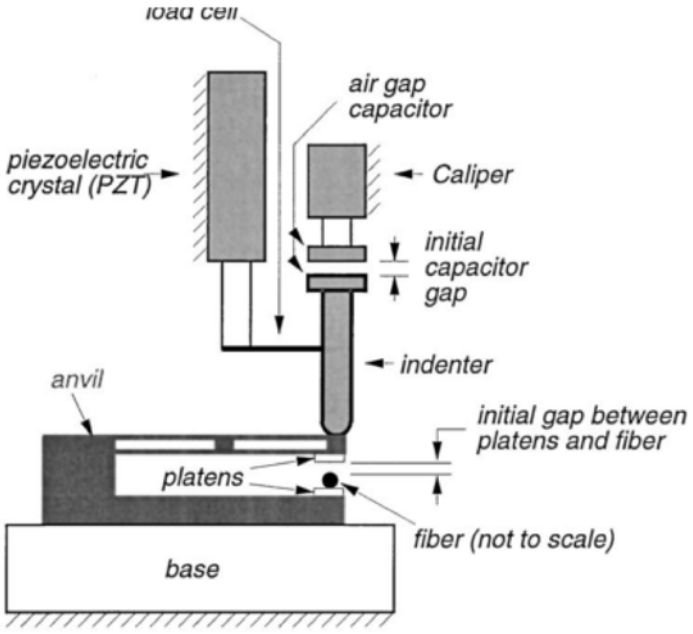

Figure 1.9. Automated transverse compression setup by Singletary and Davis. The setup uses a piezoelectric crystal to indent the fiber, with the corresponding displacement and compressive load measured by the air gap capacitor and load cell respectively [14].

Given the high precision of these new experimental setups, fibers of smaller diameters can be tested, in contrast to earlier apparatus where fiber diameters were typically in the order of tens of microns [16, 17].

1.2.5 Multiple Fiber Compression

These single-fiber transverse compression setups dealt with the transverse compression of a single fiber, although the methodologies each present unique constraints

and difficulties. Due to their low compliance per unit length and the short range (approximately 0.5 to 1.0 μm) of initial elastic deformation during compression, the initial elastic response is extremely sensitive to any platen surface roughness, non-parallel compression as shown in Figure 1.10, or any variations in fiber diameters.

In light of the above-mentioned issues with single-fiber setups, Phoenix and Skelton [20] performed experiments on the transverse compression of multiple fibers (one to four fibers), specifically for graphite, nylon, polyester, Kevlar 29, and Kevlar 49 fibers. The advantage of compressing multiple fibers is its relative insensitivity to non-parallel compression, and any asperities on the platen surfaces have less significant effect on the compression of the fibers. In spite of these advantages, the transverse compression of multiple fibers also presents its own set of problems. Because the tallest fibers may be compressed initially as the top platen moves downward, this results in a low estimated transverse fiber modulus due to inaccurately low initial compression loads as the calculation of the compressive force is divided by the total gage length.

1.3 Objective of Study

The fibers compressed in this study were Kevlar KM2 and Dyneema SK76, two of the most popular high-performance fibers in the industry today. The transverse compression setup from previous literature was improved upon and a twin-fiber experimental setup was built to address the aforementioned problems with aforementioned setups. The misalignment in fibers during compression due to microscopic asperities and tilting results in an inaccurate measurement of the nominal stress-strain response (Figure 1.10).

While multiple fibers, as previously mentioned, show inaccuracies in the initial portion of transverse compression due to the slight difference in fiber diameters, in this novel twin-fiber compression setup, the top platen is first laid across the fibers,

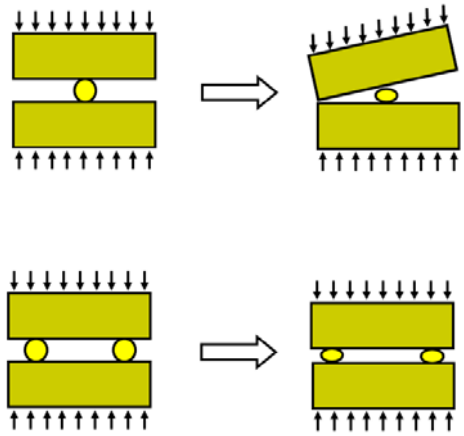

Figure 1.10. Misalignment of top and bottom platens during a transverse compression experiment for single-fiber setup (top) and proper contact of fibers and platen for twin-fiber transverse compression (bottom).

ensuring that the fibers always remains in contact with the platen and the force applied is directed through the center of the fibers.

The second motivation of this study is to transversely compress these fibers to much higher strains. Previous studies have aimed to characterize and obtain a value for the transverse modulus, and therefore very few studies exist which go to strain values beyond the elastic region of deformation. In typical ballistic applications, these fibers undergo extremely high-strain deformation.

Finally, in order to delineate the rate effects of these fibers under transverse compression, the quasi-static results were also compared to high-rate experimental results. These high-rate experiments were performed using a miniature Kolsky bar, with a transmitter bar of diameter 127 μm, which presses on a single fiber transversely at a strain rate of $5 \times 10^6 s^{-1}$. The significance of high-rate transverse mechanical responses is apparent, as these fibers are typically used in scenarios where high-rate deformation is the norm, especially in ballistic applications.

2. Experimental Methodology

2.1 Sample Preparation

The materials used in this study were Kevlar KM2 fibers and Dyneema SK76 fibers, as these fibers have been previously characterized and therefore provide a reference value for calibration. An analysis performed using a scanning electronic microscope of the pre-compressed fibers show relatively consistent diameters through the compression range, and measurement using these images gives average diameters of approximately 12 μm for the Kevlar KM2 fibers and 16 μm for the Dyneema SK76 fibers.

2.2 Quasi-Static Experimental Setup

2.2.1 Sample mounting

The fibers were laid parallel on the bottom platen using a cardboard sample holder shown in Figure 2.1, with a gage length of 9 mm per fiber and spaced 1 cm apart. Some slack was allowed in the fiber samples during preparation to reduce the possible effects of putting the samples in slight pre-tension, as this may possibly affect the transverse compression results. It is imperative to ensure the fibers are mounted on

Table 2.1 Properties of Kevlar KM2 and Dyneema SK76 fibers.

Fiber	Kevlar KM2	Dyneema SK76
Diameter [μm]	12.02±0.32	15.94±0.27
Longitudinal Modulus [GPa]	84.62 ± 4.18 [21]	120 [22, 23]

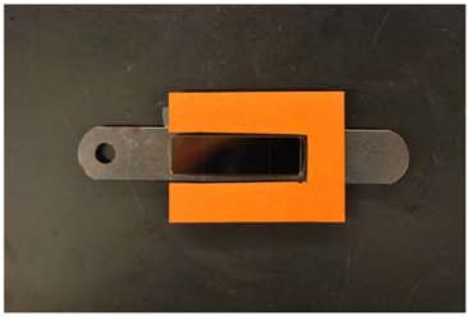

Figure 2.1. Cardboard sample holder used in experiment. Fiber samples are mounted width-wise with a gage length of 9 mm each.

the sample holders such that they are still parallel when laid on the bottom platen without causing any unnecessary tensile stress in the fibers.

2.2.2 Transverse compression setup with piezo-electric actuator

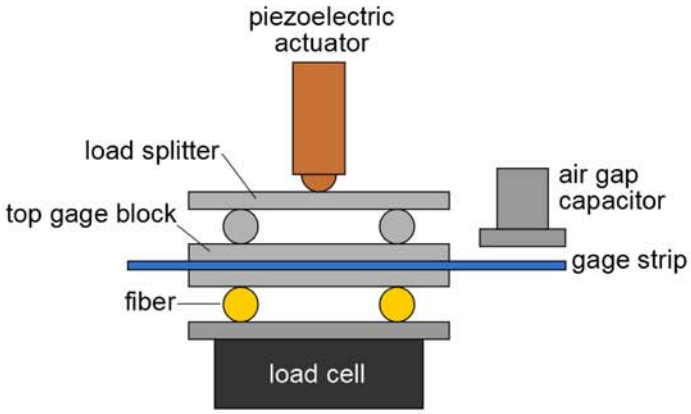

Figure 2.2. Schematic of twin-fiber transverse compression experimental setup.

A schematic of the compression setup is shown in Figure 2.2. The top platen comprises two tool steel gage blocks with a steel gage strip sandwiched in between. The gage blocks and gage strip were then securely clamped together and bonded using J-B Weld Steel Reinforced epoxy to minimize any gaps at the interfaces. The gage blocks used were Mitutoyo tool steel gage blocks, as they have a high modulus and are

pre-polished to a mirror finish with minimal surface roughness, which is important in ensuring proper contact with the fibers as previously explained. The gage blocks are of 9 mm width, giving a total fiber compression length of 1.8 cm.

Figure 2.3. Twin-fiber transverse compression setup using PI P840.6B piezoelectric actuator.

A Kistler 50-lb rating load cell (Kistler 9712B50) was mounted below the bottom gage block platen to measure the compressive load applied by the piezoelectric actuator (Physik Instrumente P840.6B), which has a maximum pushing load of 1000N and a total uni-axial travel of 90 μm. As the fibers get compressed, the air-gap capacitive displacement sensor (Physik Instrumente D-510.050, maximum resolution 2 nm) measures the displacement of the tool steel gage strip.

A load splitter was also designed using a Mitutoyo tool steel gage block and two 1 mm-diameter stainless steel dowel pins. The dowel pins of were spaced 1 cm apart and glued on the gage block surface using J-B Weld Steel Reinforced Epoxy. The function of the load splitter is to ensure that the loads are applied directly and evenly above the two fibers, as well as prevent beam deflection from the flexing of the gage strip, which may otherwise result in an inaccurate displacement measurement.

The cyclic transverse compression experiments were performed at a strain rate of 0.02/s, with a maximum targeted nominal strain (based on the initial fiber diameter) of 80%. The cycle was controlled using a function generator with a sawtooth signal, and the output displacement and load signals were recorded using a Tektronix oscilloscope.

2.2.3 Modified transverse compression setup with steel rod compressor

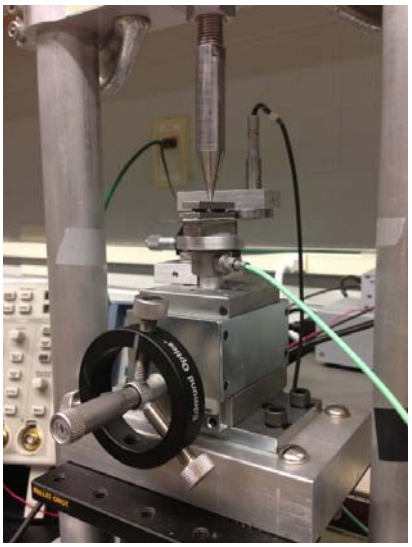

Figure 2.4. Modified transverse compression setup for manual adjustment of vertical stage displacement.

During the course of compression, it was found that the piezo-electric actuator was unable to compress the fibers sufficiently, as the maximum nominal strain achieved using the piezo-electric actuator setup was approximately 20-30% for both fiber types, way below the target nominal strain of about 70-80%. A modification was therefore made by replacing the actuator with an A2 tool steel rod (Rockwell C 62) with a rounded tip of the same diameter as the P840.6B piezoelectric actuator, the exact dimensions of which are included in the appendix.

The vertical translation of the bottom stage (resolution 1 μm) was then manually adjusted in order to compress the fibers to larger transverse nominal strains. The modified setup is shown in Figure 2.4.

2.2.4 Counter-Intuitive Nominal Stress-Strain Response

Due to inevitable irregularities of the fibers as well as minor misalignment in the setup due to the small length scale of the fibers compared to the apparatus, counter-intuitive stress-strain responses may arise in cases where one fiber gets compressed before the other. This response is easily identified during the compression cycle, as the displacement measured by the air gap capacitor exhibits very high deflection of several diameters in the initial compression region as it pivots about one of the fibers due to misalignment.

While these experimental curves are still recorded nonetheless, they are only examined qualitatively to demonstrate the existence of such an avoidable phenomenon and not included in the final obtained stress-strain response of the fibers. In light of this, the fibers were tested until at least 25 appropriately-compressed samples were obtained.

2.3 Calibration of Experimental Setup

2.3.1 System compliance

The existence of system compliance is an unavoidable phenomenon that arises because of any slight gaps or irregularities at the epoxy bonding surfaces, as well as deformation of the components within the system such as the translation stages and tool steel blocks. Due to the very small length scale of the experiments, it is necessary to experimentally determine the system compliance of this setup as it undergoes compressive stress, as even a slight system deformation of 1 μm may result in an incorrect deformation value of up to 10%.

The system was loaded without any fiber samples to determine the amount of deformation within the loading range. This system compliance is then subtracted from the raw displacement data to obtain the actual fiber compression. The raw system compliance data is given in Figure 2.5 below.

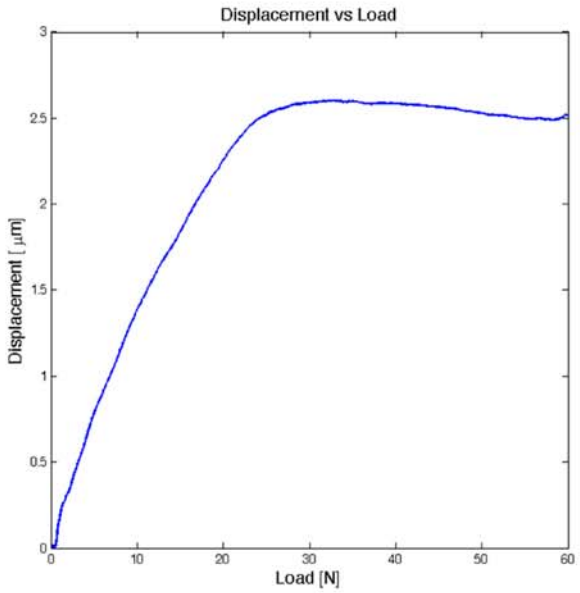

Figure 2.5. System compliance plot of modified transverse compression setup with A2 tool steel compressing rod.

2.4 Scanning Electron Microscopy

In order to verify the proper compression of the fibers, scanning electron microscopy was used to determine the length of the compressed zone as well as the final compressed width of the fibers. Post-compression, the fibers were removed from the cardboard substrate carefully and mounted parallel to each other on a separate piece of substrate..

The fibers and aluminum block were subsequently coated with palladium-gold using a Hummer 6.2 sputter coating machine before being inspected under a scanning electron microscope (FEI Nova 200 NanoLab DualBeamTM-SEM/FIB and Hitachi

S-4800 Field Emission SEM) in Birck Nanotechnology Center. The coating is several orders of magnitude smaller than the nominal diameters of the fibers, and therefore do not affect the dimensions significantly when viewed under the SEM. The compressed lengths of the fibers were calculated by obtaining the coordinates of both ends of the compression zone, and then calculating the distance between the coordinates.

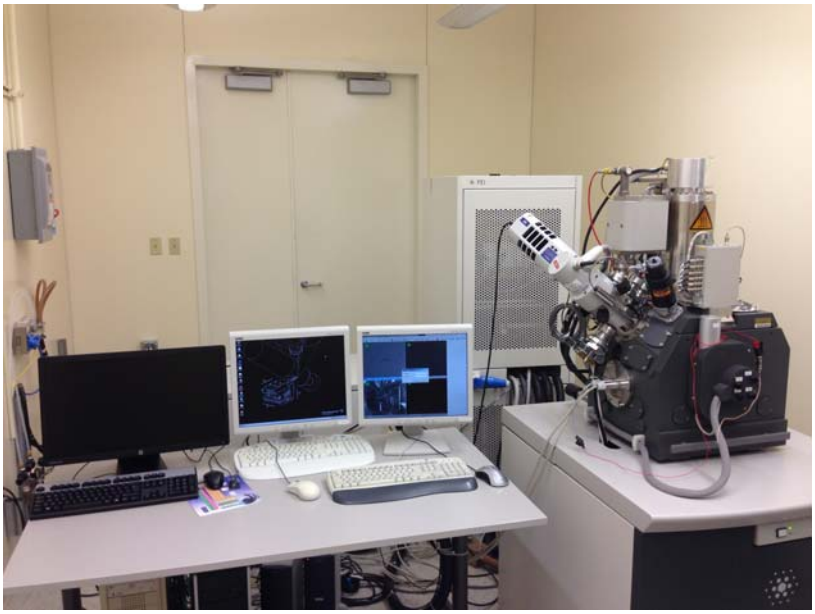

Figure 2.6. FEI Nova 200 NanoLab DualBeamTM-SEM/FIB in Birck Nanotechnology Center.

2.5 High-Rate Transverse Compression

In collaboration with Dr. Daniel Casem from the Army Research Laboratories, the Kevlar KM2 and Dyneema SK76 fibers were first prepared in Purdue University's Impact Science Laboratory before being tested under high-rate transverse compression using Dr. Casem's miniature Kolsky bar setup [24–26]. The apparatus works based on the same principles as a regular Kolsky bar (Figure 2.7), but due to the small length-scales of the setup, a transverse displacement interferometer (TDI) was

used on the incident bar (Figure 2.8 and a normal displacement interferometer (NDI) was used on the transmission bar (Figure 2.9) in lieu of strain gages.

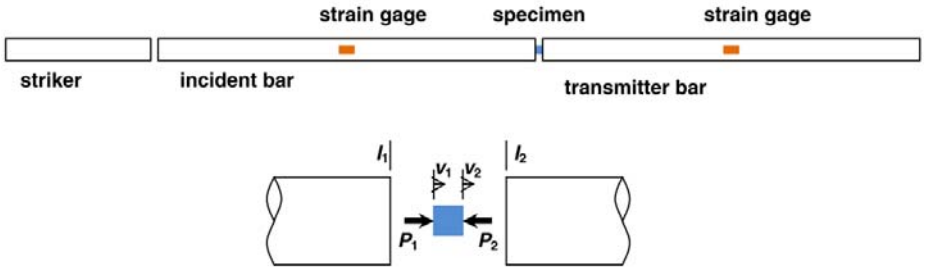

Figure 2.7. Basic schematic of Kolsky bar setup. [24].

The TDI works using a diffraction grating etched directly on the incident bar at the midpoint along its length. As the wave propagates longitudinally within the incident bar, the interference phase shift is detected by the detectors. The displacement and velocity of the incident bar can be calculated from there. In order to eliminate the effects of bending waves which may arise due to slight misalignment (which significantly affects results adversely especially at very small length scales), TDIs were also used to cancel out the bending wave effects [26].

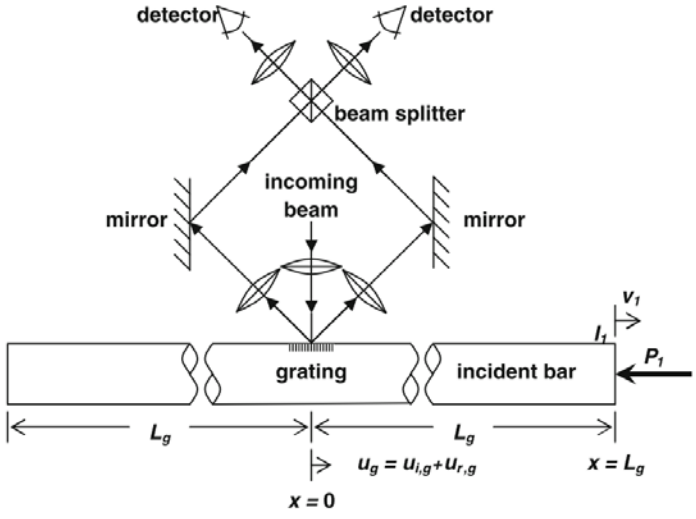

Figure 2.8. TDI used on incident bar of miniature Kolsky bar [24].

For the transmission bar, an NDI was used instead of a TDI. While it is still possible to use a TDI to measure the displacement and velocity of the bar, the NDI offers the advantage of not requiring a diffraction grating to be etched on the bar. The displacement is therefore easily measured by the NDI at the free end of the bar, provided it is polished enough to a suitable reflective finish. In contrast with the TDI, the NDI measures the phase shift in the leg of the moving mirror, producing interference fringes which can subsequently be detected at the detectors. The corresponding displacement and velocity can then be calculated.

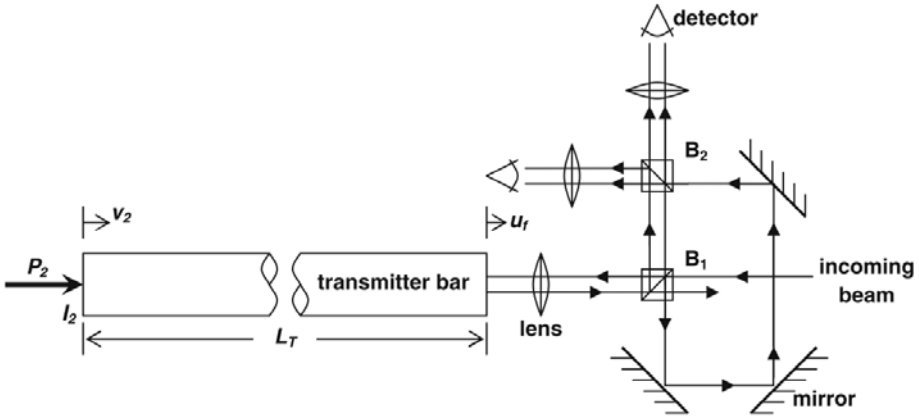

Figure 2.9. NDI used on transmission bar of miniature Kolsky bar [24].

Initially, experiments were conducted with stainless steel bars with diameters of 794 μm, 50 mm in length. Optical instrumentation was used to avoid difficulties associated with strain gages on bars of this size. However, it was found that the transmitted signal was too small to reliably measure the force developed in the fibers, even when multiple fibers were tested simultaneously. For this reason, the transmitter bar was replaced with a smaller diameter (127 μm) steel bar while the original incident bar (794 μm diameter) was maintained. Even though this change required a reduction in specimen length, the corresponding reduction in area of the transmitter bar increased the magnitude of the transmitted pulse to measureable levels. The loading surface of each bar was polished to a 0.04 μm finish, and specimens were

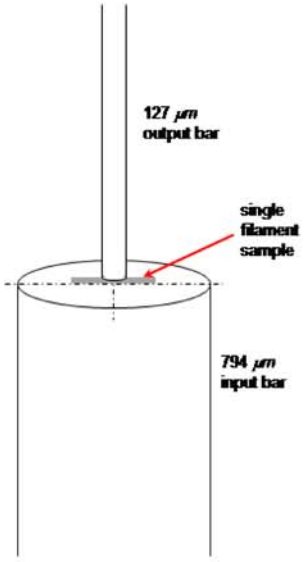

Figure 2.10. A Kolsky bar set-up for high-rate transverse compression. A smaller diameter transmitter bar is used to increase sensitivity of the force measurement.

loaded (without lubrication) along a diameter of the smaller bar. This is shown in Figure 2.10.

In this way, the compressed length of each fiber is 127 μm. Total fiber lengths range from 0.5 to 0.8 mm. It is assumed that the uncompressed portion of each fiber has negligible effect on the measured force displacement curves, although clearly the specimens are "pinched" at the circumference of the transmitter bar.

3. Results & Discussion

The corresponding nominal stress and nominal strain of each cycle was calculated using Equations 3.1 and 3.2, where F is the total compressive load applied, L is the total compression length given as 1.8 cm, d is the average fiber diameter, and δd is the measured transverse fiber deformation (after accounting for system compliance). The nominal values facilitate the calculations of the transverse stress and strain, which would otherwise involve an in-depth consideration of the actual current shape of the fiber cross-section.

$$\sigma_{nom} = \frac{F}{L \times d} \tag{3.1}$$

$$\varepsilon_{nom} = \frac{\Delta d}{d} \tag{3.2}$$

It is important to note that while this setup solves the problem of the tallest fiber being compressed first, the fibers will inherently experience slight pre-loading when the top platen is placed on the fibers prior to the compression cycle. Further calculation and verification in the sections below reveals that this pre-stress is negligible and will not result in significant deviation.

The main assumption in calculating this pre-strain is that the elastic transverse moduli of KM29 and KM2 are within the same order of magnitude; however, the pre-strain experienced by the fibers for subsequent tests can be assumed to be negligible, as long as the fiber transverse moduli remain to be within the same order of magnitude of KM29 and KM2. The SK76 fibers were compressed in the same manner as the KM2 fibers.

3.1 Quasi-static transverse compression results

3.1.1 Gold fiber calibration

Hard temper gold fibers of 99.9% purity and 10 μm diameter (obtained from Goodfellow® USA) were put under transverse compression to calibrate the system. Gold is used as a calibration material due to its isotropic properties. As the stress-strain data for pure gold was not readily available, material characterization was performed to obtain a stress-strain curve to be input into the ABAQUS FE model. The gold fibers were tested in tension using the MTS 810 system at a nominal strain rate of 0.01/s. The samples had a gage length of 5.56 mm and attached on to a cardboard substrate using J-B Weld Steel Reinforced Epoxy as per the ASTM standard procedure (C1577-03). The load was measured using a quartz force transducer (Kistler 9712B50), and the engineering stress-strain curves were subsequently obtained from a total of 6 gold fiber samples as shown in Figure 3.1.

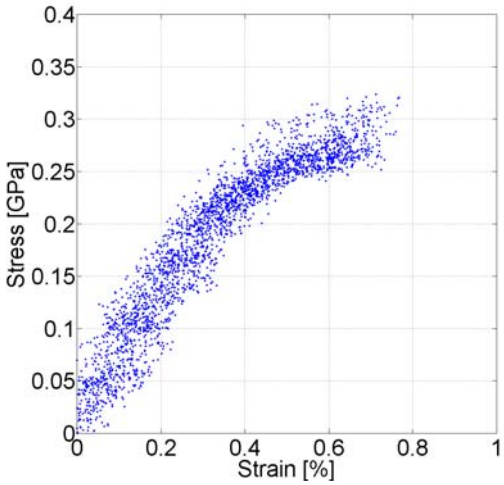

Figure 3.1. Engineering stress-strain curve for tensile loading gold fibers of purity 99.9% and diameter 10 μm.

From the stress-strain curve obtained for the gold fibers, the gold fibers had a tensional modulus of 77.5 GPa, a yield strength of approximately 225 MPa at 0.4% strain.

Given that the total weight of the top platen and gage strip piece is 0.283 g, the amount of pre-stress applied on the two fibers is 1.31 MPa for a fiber diameter of 10 μm. Since gold is an isotropic material, we can assume the transverse modulus is the same as its tensile modulus. Using Hooke's Law for material constants as per Equation 3.3

$$\sigma = E\varepsilon \tag{3.3}$$

where E is the Young's modulus, a simple calculation for the gold fibers gives us a pre-strain value of 1.66×10^{-5}, which is on a negligible order of magnitude compared to the experimental nominal strain values. This assumption also implies that as long as the transverse moduli of the sample material is on the order of 10^9 Pa, the pre-strain due to the top gage block piece is negligible.

Similarly, a maximum strain of 80% was targeted, although experimentally these strains could not be achieved due to mechanical limitations of the equipment. A maximum strain of approximately 45% was achieved instead. The obtained stress-strain results and deviation are shown along with the ABAQUS FE analysis results in Figure 3.4.

Gold fiber finite-element analysis

To further verify the results of the gold fiber calibration, a finite-element analysis was performed using ABAQUS/Explicit (v 6.12). The obtained stress-strain properties up to the yield stress were then input into the commercial software package ABAQUS/Explicit using a elastic-plastic material model, with the obtained experimental elastic modulus of 77.5 GPa and Poisson's ratio of 0.44. A 2D plane strain model was used to reduce the required number of elements, and the top and bottom platens were assumed to be rigid and undeformable. The friction coefficient between gold and tool steel were unknown, and therefore the values tested were 0.01, 0.1, 0.25 and 0.5. Convergence studies using a coarse mesh with 450 linear elements and a

fine mesh with 15,973 linear elements (Figure 3.2) show that a coarse mesh was sufficiently accurate with a difference of 0.1% at the compression strain levels required. However, the elements near the center of the coarse mesh became relatively distorted due to the high compressive strain levels, therefore the fine mesh with a higher mesh density in the center was preferred.

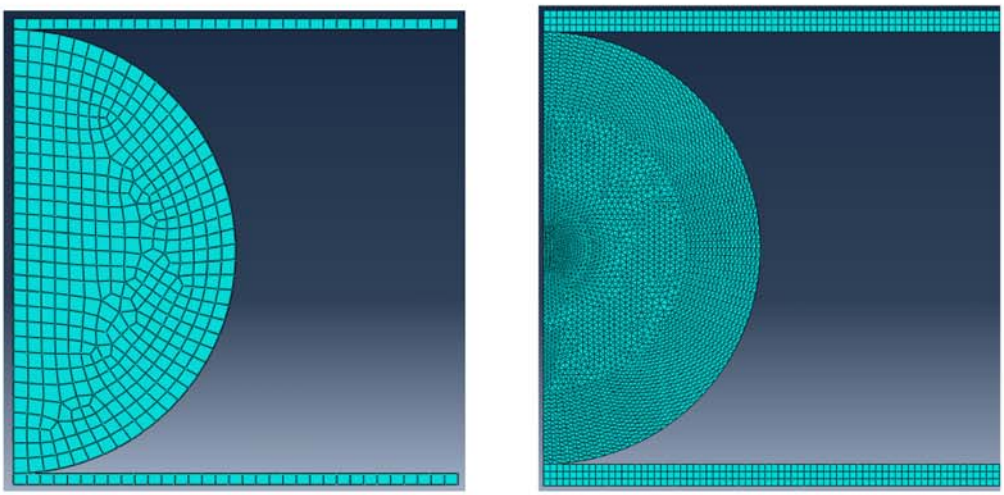

(a) (b)

Figure 3.2. ABAQUS finite element mesh used for convergence study. Figure (a) shows the coarse mesh with 450 elements, and Figure (b) shows the fine mesh with 15,973 elements.

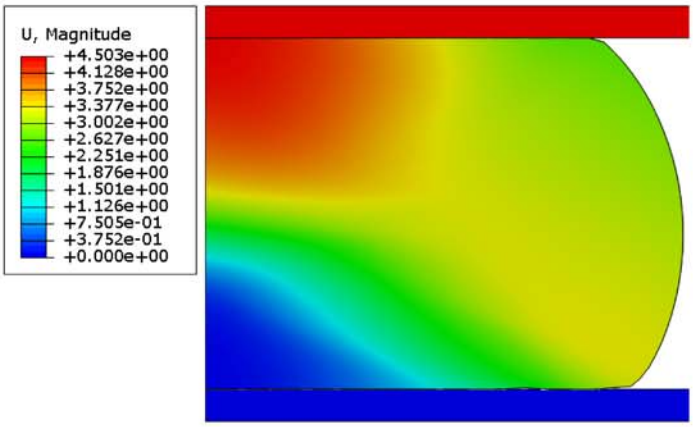

Figure 3.3. Post-compression of gold fiber from FE analysis using ABAQUS/Explicit.

The post-compression width of the FE simulation was 16.5876 μm at a nominal compressive strain of 45%. The obtained nominal stress-strain curves were subsequently obtained for the above-mentioned friction coefficients and compared to the experimental compression of the gold fiber samples.

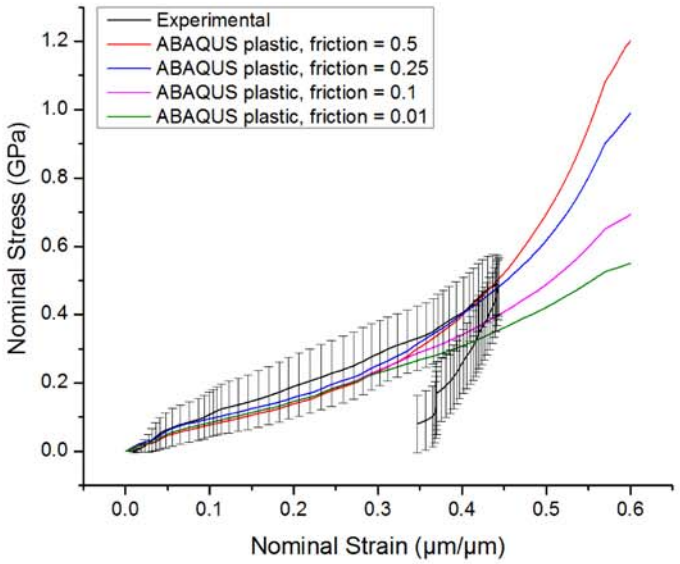

Figure 3.4. Comparison of post-compression of gold fiber from FE analysis using ABAQUS/Explicit.

The obtained experimental results line up very well with the finite element simulation results, especially for a friction coefficient between gold and tool steel of 0.25 and 0.5.

Verification using scanning electron microscopy

To verify the post-compression results of the transverse compression setup, the compressed gold fibers were then put under a scanning electron microscope to determine the total compressed length and width to ensure that uniform and proper compression was achieved experimentally.

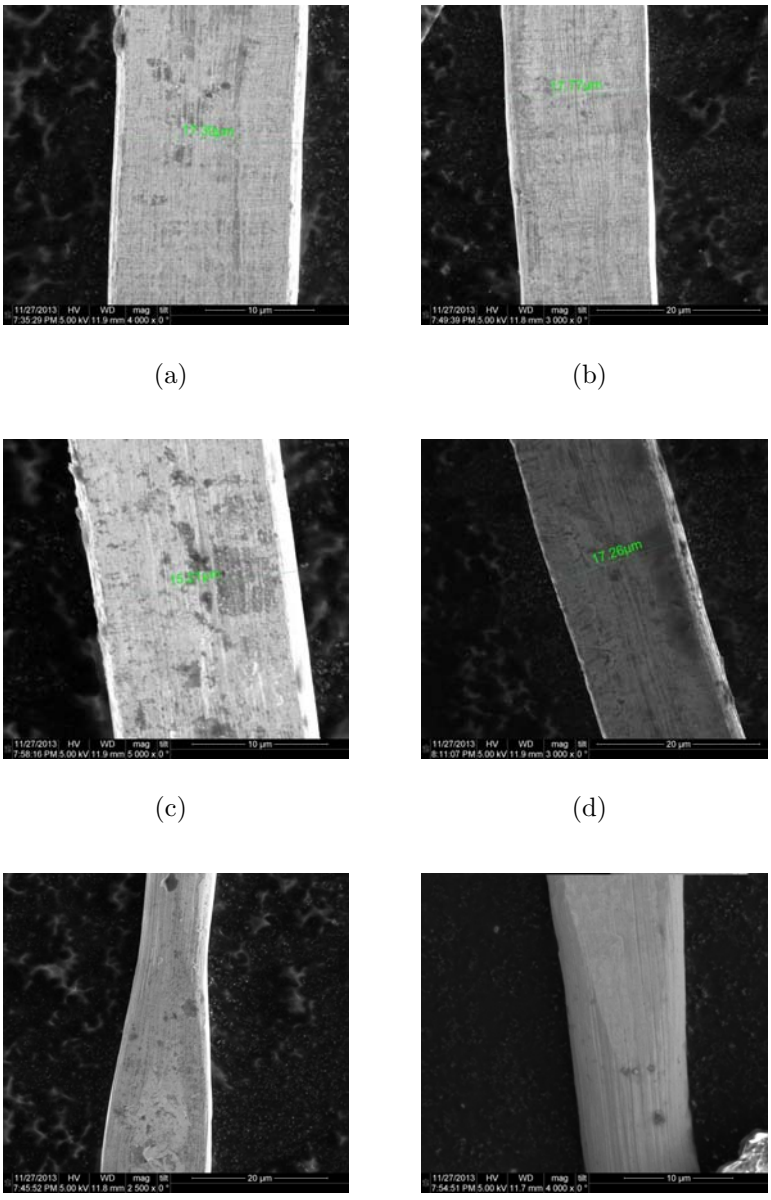

(a) (b)

(c) (d)

(e) (f)

Figure 3.5. Scanning electron microscope images for post-compression gold fibers. Figures (e) and (f) show the end effects of transverse compression.

The effects of the slightly-rounded platen edge can be observed in Figure 3.5(e) and (f), where the end of the compression zone transitions to the uncompressed zone with a sort of chamfer. However, the gage length of the fibers is long enough for these compression end-zone effects to be negligible in determining the nominal stress-strain values. The average compression zone length is 8.54 mm and the average post-compression width is 16.37 μm.

The average post-compression length of the gold fibers is 8.54 mm compared to an experimental gage length of 9 mm. This slight deviation can be attributed to the fact that the samples are not exactly aligned straight when put under the SEM, and therefore a shorter length is calculated.

3.2 High-rate transverse compression results

Figure 3.6 shows the incident, reflected, and transmitted pulses for a typical experiment on a Dyneema® filament. The force-displacement curve is shown in Figure 3.7. Also shown is the deformation rate, which typically reaches between 12 and 13 m/s for the filament experiments. Note that most of this deformation occurs during the first 2 μs of the loading; because of the relatively large diameter of the incident bar, the rate is ramped. Also note the load measurement is made during the rising portion of the transmitted pulse. This signal is obtained from a reasonable number of interference fringes from the NDI (approximately 12) —a portion of which is shown in Figure 3.8.

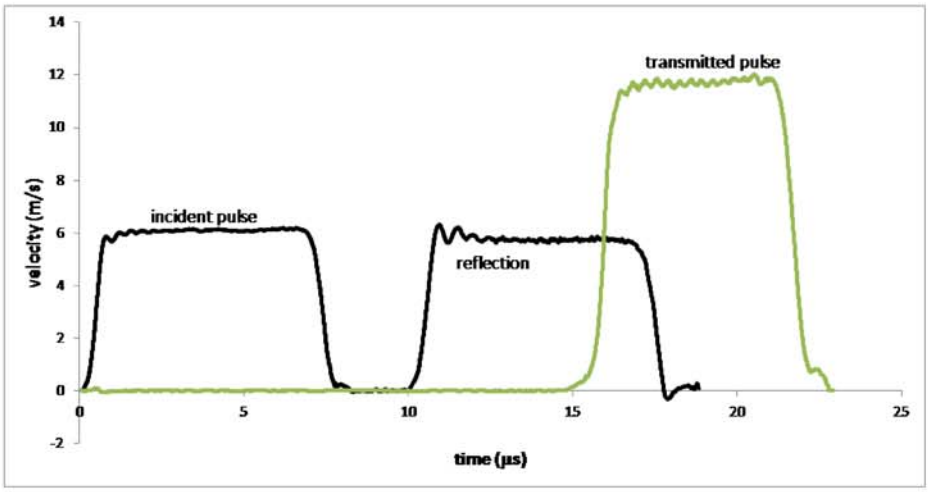

Figure 3.6. Typical pulses measured from the arrangement shown in Figure 2.10. Note they are reported in terms of particle velocity, rather than the more commonly-used strain.

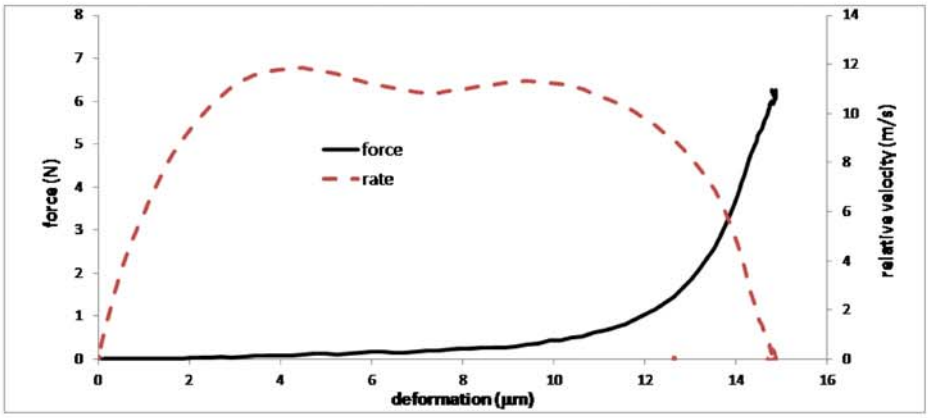

Figure 3.7. Force-displacement (or deformation) curves for high-rate compression.

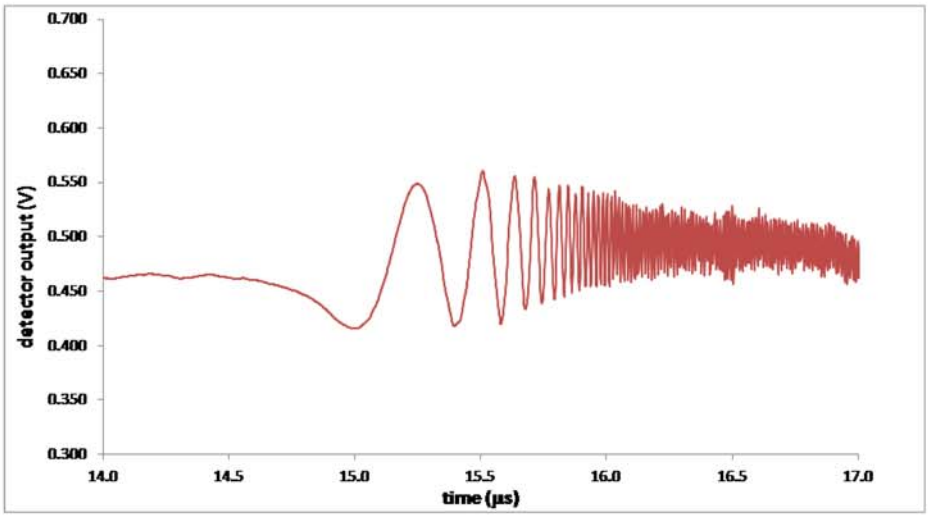

Figure 3.8. Example interference fringes from the NDI. About the first 10-12 fringes are relevant to the deformation of the fiber, sufficient for a reliable force measurement.

Using the force-deformation data obtained as per Figure 3.7, the nominal stress-strain curves for KM2 and SK76 were obtained using Equations 3.1 and 3.2, similar to the quasi-static results.

3.3 Kevlar® KM2 transverse compression results

By using Singletary's previously-obtained elastic Young's modulus value of 2.59 GPa for KM29 fibers [14], the initial transverse nominal pre-strain of the fiber was approximated to be 5.06×10^{-4}, again a negligible pre-strain value. The nominal stress-strain curves for both quasi-static and high-rate transverse compression experiments were superposed and compared, as in Figure 3.9.

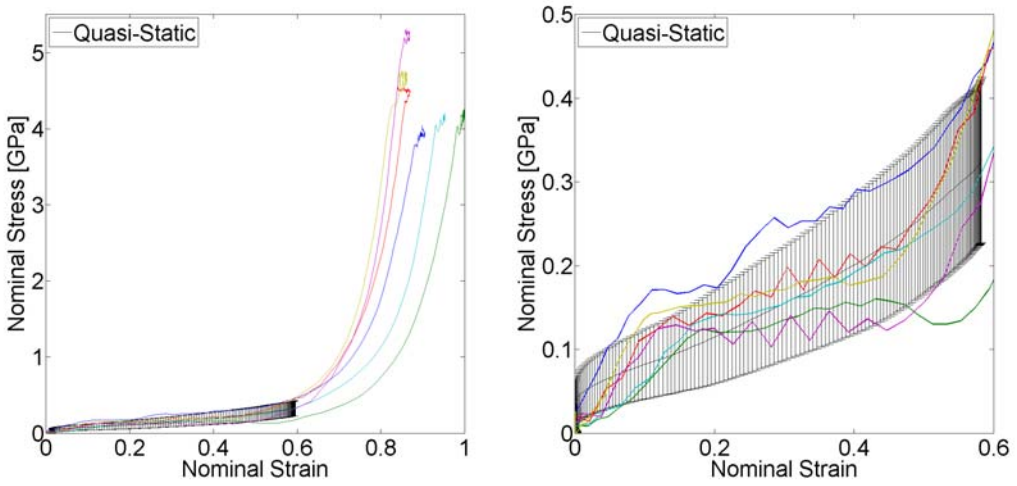

(a) (b)

Figure 3.9. Comparison of quasi-static and high-rate transverse compression of Kevlar® KM2 fibers. Figure (b) shows the zoomed-in curves

The high-rate compression results obtained by Dr. Daniel Casem (Army Research Laboratory) were subsequently compared to the obtained quasi-static twin-fiber compression results. It is interesting to note that the initial stress-strain curves line up with very little deviation; however, this does not imply that there are no rate effects when polymer fibers are compressed transversely. When zoomed in to the low strain portion of the curves, the high-rate and quasi-static curves appear to deviate slightly. Currently, there is insufficient high-rate data to form a conclusion.

At a nominal strain value of approximately 60%, no further observable deformation of the fiber was seen during the quasi-static compression cycle. On the other hand, the high-rate compression results achieved a maximum nominal strain of approximately 90%. This difference in maximum nominal strain at different compressive strain rates is due to the physical limitations of the quasi-static twin-fiber setup. A larger amount of force is required to increase the strain in the fiber as it becomes flatter and more ribbon-like. Even though the nominal stress is calculated based on the original

diameter of the fiber, the actual cross-sectional geometry has changed drastically, resulting in extremely high stresses required to compress the fiber further.

It should also be noted that the high-rate curves appear to be slightly translated along the x-axis. The slight shift is due to the initial displacement of the incident bar which was adjusted by hand, which might have resulted in different initial strain values. To demonstrate the similarity of these curves, the high-rate curves were adjusted as in Figure 3.10.

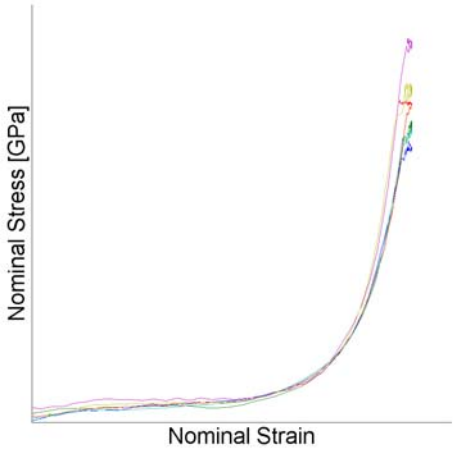

Figure 3.10. Strain-adjusted high-rate transverse compression curves for Kevlar® KM2.

3.3.1 Verification using scanning electron microscopy (SEM)

In the experiments, the maximum achieved strain using the manual compression setup was approximately 58% for the KM2 fibers. The compressed KM2 fibers had an average maximum nominal stress of 285 MPa at a maximum nominal strain of 58% after accounting for system compliance. To verify that the fibers underwent proper transverse compression, the post-compression fibers were examined using a scanning electron microscope. The examined KM2 fibers had an average post-compression width of 21.36 μm over a total compressed length of 8.48 mm. The effects of the

rounded platen edge can be observed in Figure 3.11(e) and (f), however the sample length of the fibers is long enough for these compression end-zone effects to be negligible.

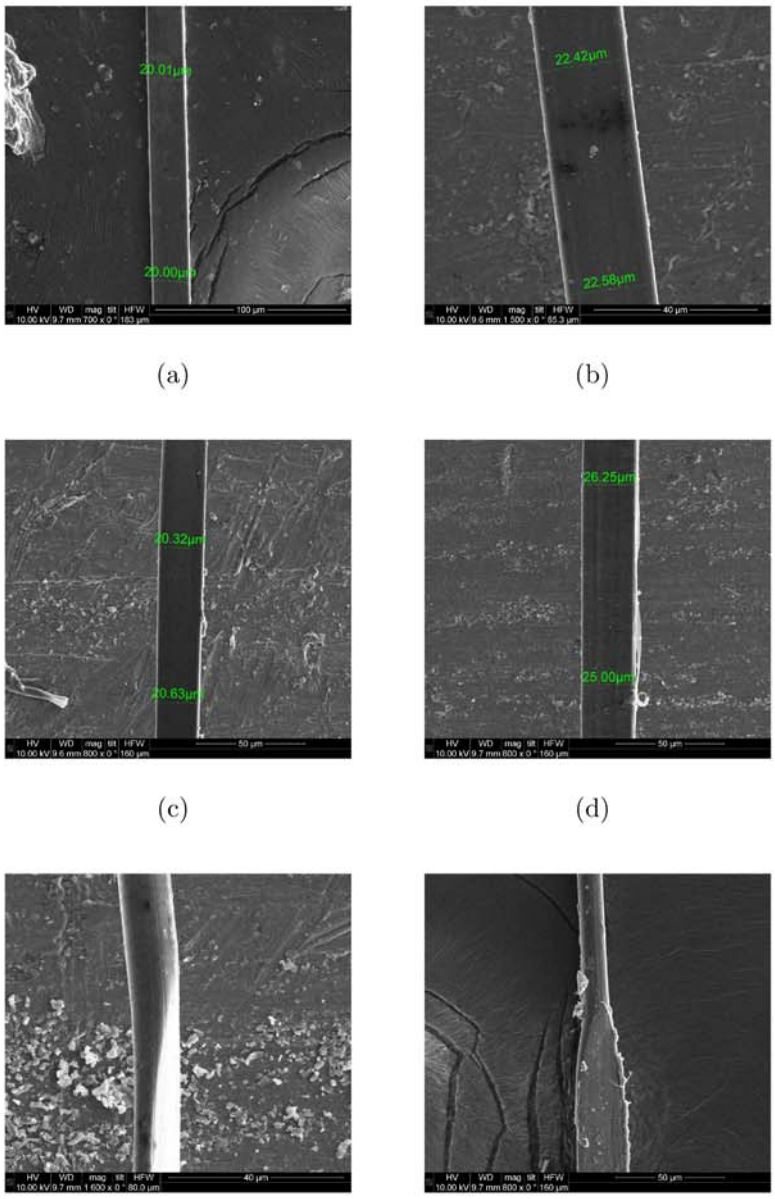

(a) (b)

(c) (d)

(e) (f)

Figure 3.11. Scanning electron microscope images for post-compression KM2 fibers. Figures (e) and (f) show the end effects of transverse compression.

3.4 Dyneema® SK76 transverse compression results

The pre-strain value of Dyneema could not be readily calculated due to lack of information regarding the transverse modulus of Dyneema SK76 fibers. However, it is not far-fetched to assume that the transverse modulus of Dyneema SK76 is on the same order of magnitude, if not larger, compared to that of the gold fibers. This means that the pre-strain is on a negligible order of magnitude, as with the KM2 and gold fibers. The nominal stress-strain curves for both quasi-static and high-rate transverse compression experiments were superposed and compared, as in Figure 3.12.

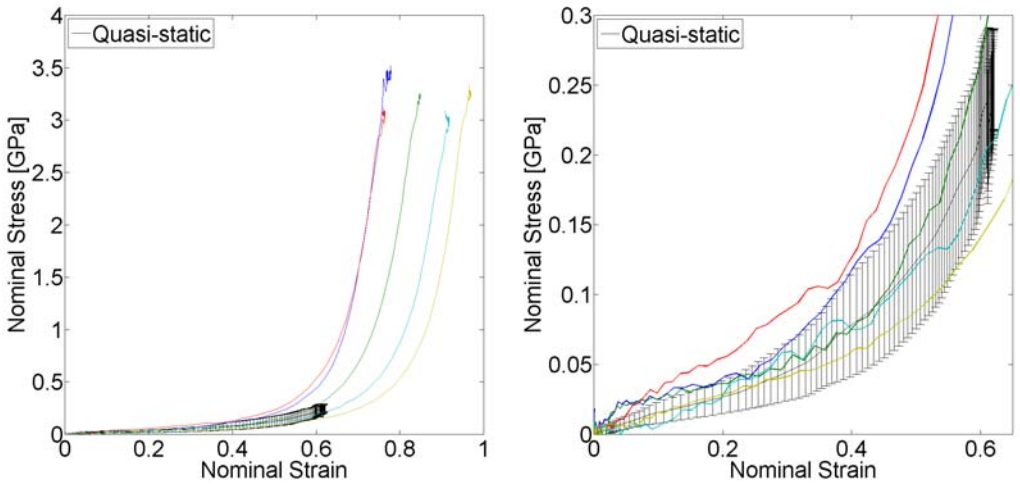

(a) (b)

Figure 3.12. Comparison of quasi-static and high-rate transverse compression of Dyneema® SK76 fibers. Figure (b) shows the zoomed-in curves

Similarly, the high-rate compression results obtained by Dr. Daniel Casem were compared to the obtained quasi-static twin-fiber compression results. As with the Kevlar KM2 fibers, the initial stress-strain curves of Dyneema SK76 line up in the initial portion as well. The high-rate compression results achieved a maximum nominal strain of approximately 61%. The sudden increase in nominal stress is also observable for Dyneema SK76 past a nominal strain value of approximately 50%.

As with the KM2 fibers, the high-rate results appear to be slightly translated along the x-axis. The high-rate curves were therefore strain-adjusted to demonstrate their similarity, as in Figure 3.13.

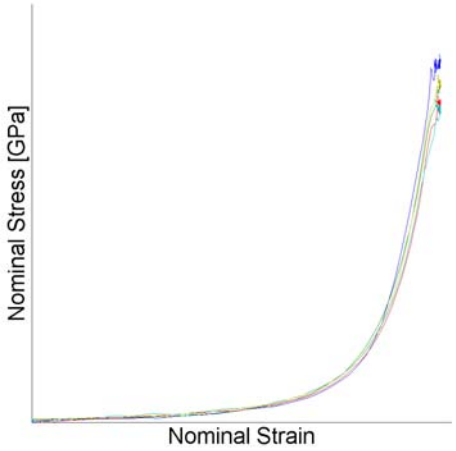

Figure 3.13. Strain-adjusted high-rate transverse compression curves for Dyneema® SK76.

3.4.1 Verification using scanning electron microscopy (SEM)

In the experiments, the maximum achieved strain using the manual compression setup was approximately 61% for the Dyneema SK76 fibers. The compressed fibers had an average maximum nominal stress of 285 MPa at a maximum nominal strain of 61% after accounting for system compliance. The post-compression fibers were again examined using a scanning electron microscope.

The examined SK76 fibers had an average post-compression width of 40.99 μm over a total compressed length of 8.34 mm. The effects of the rounded platen edge can be observed in Figure 3.14(e), where the end of the compression zone transitions to the uncompressed zone with a chamfer, similar to the previous two compressed fibers. Again, the sample length of the fibers is long enough for these compression end-zone effects to be negligible. The compression zone length of Dyneema is slightly shorter

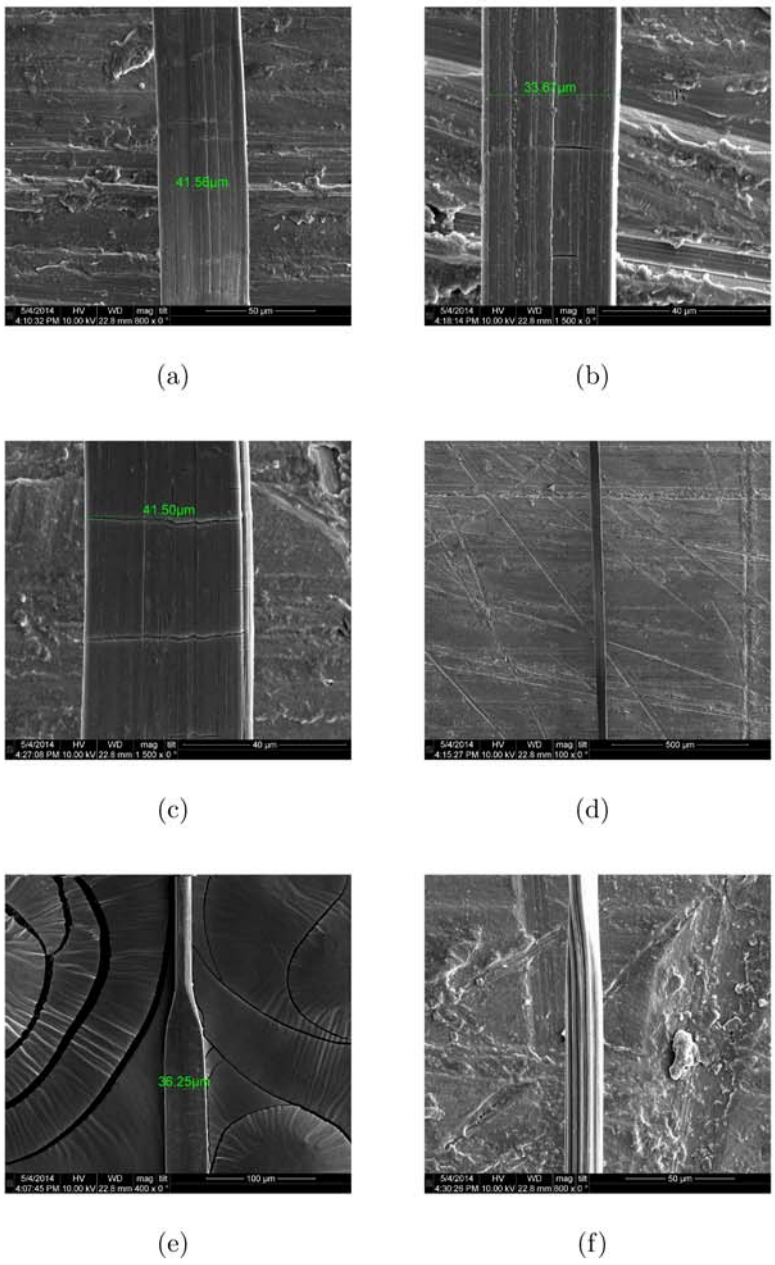

Figure 3.14. Scanning electron microscope images for post-compression SK76 fibers. The fibrils can be clearly seen in post- and pre-compression in (b) and (e) respectively.

than gold or KM2 due to a large amount of twist when mounting the post-compression fibers for SEM imaging.

Figure 3.14(d) shows the uniform compression of the fibers over the whole gage length. It is interesting to note that the fibrils are clearly visible in Figures 3.14(b) and (e) in the fibers before and after compression.

3.5 Compression results of non-polymer fibers

Following the successful transverse compression of the two polymer fibers, Kevlar® KM2 and Dyneema® SK76, non-polymer fibers were also tested for their transverse mechanical response. Specifically, glass fibers were tested as they are expected to exhibit vastly different properties from polymer fibers due to their structure and brittleness. The resulting stress-strain curves are extremely counter-intuitive do not give particularly useful information, and therefore only the displacement-time curves are given below.

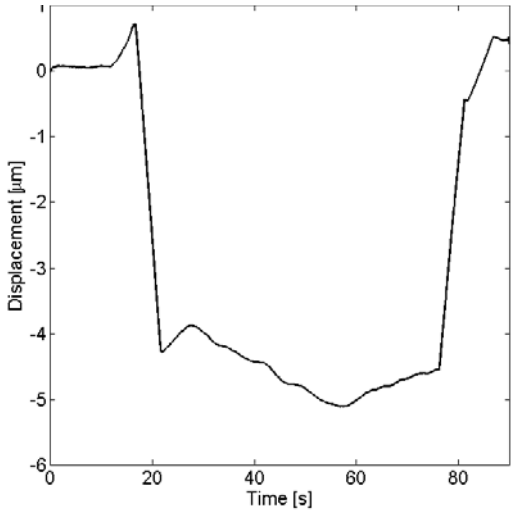

Figure 3.15. Displacement-time history for glass fiber transverse compression.

The displacement history of the glass fibers shows a slight increase in transverse deformation before the deformation abruptly and rapidly decreases, in some cases to a negative deformation value i.e. the air gap decreases with increased compressive

load. This decrease in air gap occurs when one of the fibers fails due to its brittleness, resulting in the top gage strip pivoting about the other fiber. With a further increase in compressive load, the second fiber fails in a brittle manner, resulting in a sudden increase in air gap again.

4. Conclusions

The transverse compression of anisotropic high performance ballistic fibers was performed at both quasi-static and high strain rates to determine the transverse mechanical response of these fibers and the rate effects on the mechanical behavior. A twin-fiber quasi-static transverse compression setup was designed to evenly load and deform the fiber specimen in the gage section. For high-rate transverse compression, a miniature compression Kolsky bar was used to compress a single fiber transversely at high rates. The velocities were measured using a transverse displacement interferometer and a normal displacement interferometer respectively. Using these new experimental setups, the transverse compression behavior of Kevlar® KM2 and Dyneema® SK76 fibers were characterized.

For quasi-static transverse compression, the non-linear stress-strain behavior for both fibers was recorded. Experimental calibration of the novel twin-fiber compression setup using gold fibers and finite element simulation shows good agreement between experimental and numerical simulation results. Scanning electron microscopy of the post-compression fibers further demonstrated the accuracy of the twin-fiber compression setup as well as the proper uniform compression of the fibers. However, the quasi-static setup reached maximum experimental strains due to large compressive stresses required to increase the deformation of the fibers when they are flat.

On the other hand, the resultant stress-strain behavior shows that the high-rate experiments allow the fiber to be compressed to extremely large strains, revealing a significant strain-resisting response of both fibers when the nominal strain is beyond 60% due to a change in cross-sectional geometry. After a strain level of 60%, it becomes significantly much harder to further reform the fibers, resulting in a sharp increase in nominal stress which could only be achieved via high-rate transverse compression. Comparison between the quasi-static and high-rate results shows that the

stress-strain behaviors coincide relatively closely for strains below 50%; however, further high-rate experimentation has to be performed in order to reach a conclusion regarding the rate effects of transverse compression.

Future work could include the transverse characterization of other fibers using these two novel experimental setups, as well as improving the quasi-static setup to allow for larger compressive loads. Currently, preliminary work has been done on glass fibers, which exhibit counter-intuitive stress-strain responses compared to polymer fibers due to their brittleness.

LIST OF REFERENCES

LIST OF REFERENCES

[1] José M. García, Félix C. García, Felipe Serna, and José L. de la Peña. High-performance aromatic polyamides. *Progress in Polymer Science*, 35(5):623–686, May 2010.

[2] Roelof Marissen. Design with Ultra Strong Polyethylene Fibers. *Materials Sciences and Applications*, 02(05):319–330, 2011.

[3] Jean-Baptiste Donnet. *Carbon Fibers*. CRC Press, 3rd edition, 1998.

[4] H. H. Yang. *Kevlar Aramid Fiber*. Wiley Publishing, 1993.

[5] Karl Chang. Aramid Fibers. *Materials Park, OH: ASM International*, pages 41–45, 2001.

[6] Kevlar chemical structure.

[7] George Wypych. PPTA. In *Handbook of Polymers*, pages 523–526. ChemTec Publishing, 2012.

[8] Kevlar Fibers, 2014.

[9] Menachem Lewin and Jack Preston. *High Technology Fibers: Part D*. Marcel Dekker, Inc., New York, 1996.

[10] AJ Pennings and RJ Van Der Hooft. High-speed gel-spinning of ultra-high molecular weight polyethylene. *Polymer Bulletin*, 4, 1986.

[11] Dyneema Product Grade Technical Data.

[12] DW Hadley, PR Pinnock, and IM Ward. Anisotropy in oriented fibres from synthetic polymers. *Journal of Materials Science*, 4:152–165, 1969.

[13] Valentin L. Popov. *Contact Mechanics and Friction*. Springer Berlin Heidelberg, Berlin, Heidelberg, 2010.

[14] J Singletary and H Davis. The transverse compression of PPTA fibers Part I Single fiber transverse compression testing. *Journal of Materials Science*, 5:573–581, 2000.

[15] PR Pinnock, IM Ward, and JM Wolfe. The compression of anisotropic fibre monofilaments. II. *Proceedings of the Royal Society of London. Series A, Mathematical and Physical Sciences*, 291(1425):267–278, 1966.

[16] DW Hadley, IM Ward, and J Ward. The transverse compression of anisotropic fibre monofilaments. *Proceedings of the Royal Society of London. Series A, Mathematical and Physical Sciences*, 285(1401):275–286, 1965.

[17] S. Morris. The Determination of the Lateral-Compression Modulus of Fibres. *Journal of The Textile Institute*, 39(March 2014):37–41, 1968.

[18] S Kawabata. Measurement of the transverse mechanical properties of high-performance fibres. *Journal of the Textile Institute*, 1990.

[19] Ming Cheng, Weinong Chen, and Tusit Weerasooriya. Experimental investigation of the transverse mechanical properties of a single Kevlar KM2 fiber. *International Journal of Solids and Structures*, 41(22-23):6215–6232, November 2004.

[20] S.L. Phoenix and J. Skelton. Transverse Compressive Moduli and Yield Behavior of Some Orthotropic, High-Modulus Filaments. *Textile Research Journal*, 44(12):934–940, December 1974.

[21] Ming Cheng, Weinong Chen, and Tusit Weerasooriya. Mechanical Properties of Kevlar KM2 Single Fiber. *Journal of Engineering Materials and Technology*, 127(2):197, 2005.

[22] J. W. S. Hearle. *High-Performance Fibres*. 9781855735392, 2001.

[23] K. Karthikeyan, B.P. Russell, N.a. Fleck, M. OMasta, H.N.G. Wadley, and V.S. Deshpande. The soft impact response of composite laminate beams. *International Journal of Impact Engineering*, 60:24–36, October 2013.

[24] Daniel T. Casem, S.E. Grunschel, and B.E. Schuster. Normal and Transverse Displacement Interferometers Applied to Small Diameter Kolsky Bars. *Experimental Mechanics*, 52(2):173–184, July 2011.

[25] Daniel T Casem, Stephen E Grunschel, and Brian E Schuster. Interferometric Measurement Techniques for Small Diameter Kolsky Bars. In Tom Proulx, editor, *Proceedings of the SEM Annual Conference*, volume 1 of *Conference Proceedings of the Society for Experimental Mechanics Series*, pages 463–470, New York, NY, 2011. Springer New York.

[26] Daniel T. Casem and M. B. Zellner. Kolsky Bar Wave Separation Using a Photon Doppler Velocimeter. *Experimental Mechanics*, 53(8):1467–1473, March 2013.